Measurement of the Damping of the Nuclear Shell Effect in the Doubly Magic ^{208}Pb Region

P. C. Rout,[1,2,*] D. R. Chakrabarty,[1,2] V. M. Datar,[1,2] Suresh Kumar,[1,2] E. T. Mirgule,[1] A. Mitra,[1] V. Nanal,[3] S. P. Behera,[1,2] and V. Singh[2,4]

[1]*Nuclear Physics Division, Bhabha Atomic Research Centre, Mumbai 400085, India*
[2]*Homi Bhabha National Institute, Anushaktinagar, Mumbai 400094, India*
[3]*Department of Nuclear and Atomic Physics, Tata Institute of Fundamental Research, Mumbai 400005, India*
[4]*India based Neutrino Observatory, Tata Institute of Fundamental Research, Mumbai 400005, India*

(Received 11 October 2012; revised manuscript received 24 December 2012; published 5 February 2013)

The damping of the nuclear shell effect with excitation energy has been measured through an analysis of the neutron spectra following the triton transfer in the ^{7}Li induced reaction on ^{205}Tl. The measured neutron spectra demonstrate the expected large shell correction energy for the nuclei in the vicinity of doubly magic ^{208}Pb and a small value around ^{184}W. A quantitative extraction of the allowed values of the damping parameter γ, along with those for the asymptotic nuclear level density parameter $\tilde{a}$, has been made for the first time.

DOI: 10.1103/PhysRevLett.110.062501 PACS numbers: 21.10.Ma, 24.60.Dr

The shell effect is a cornerstone of the mean field theory describing finite fermionic systems. The shell structure in atoms decides the chemical properties of the corresponding elements. In nuclear physics the spin orbit coupling, in addition, plays a dominant role in deciding the shell closures and the associated magic numbers of protons and neutrons. The nuclei having such numbers of neutrons and protons have an extra stability with respect to that expected from the average behavior described by the liquid drop model (LDM). Many important nuclear phenomena, such as the occurrence of superheavy elements [1,2], fission isomers [3,4], superdeformed nuclei [5], and new magic numbers in exotic nuclei [6,7], are the consequences of the shell effect. The shell effect also affects another fundamental property of the nucleus viz. the nuclear level density (NLD). The NLD is an indispensable input to the statistical calculation of compound nuclear decay and thus an important physical quantity for many practical applications, such as the calculations of reaction rates relevant to nuclear astrophysics, nuclear reactors, and spallation neutron sources.

The NLD was first calculated by Bethe using a noninteracting Fermi gas model, without shell effects, arriving at its leading dependence on excitation energy (E_X) and angular momentum (J) [8,9]. The generic behavior with respect to E_X is described by $e^{2\sqrt{aE_X}}$. Here, a is the NLD parameter which is related to the single particle density at the Fermi energy. Direct measurements of the NLD are based on the study of slow neutron resonances, which are mainly s and p wave, and are extrapolated to higher J values to estimate the angular momentum summed or total NLD. The total NLD inferred from such a measurement shows that on the average the level density parameter a increases linearly with the mass number (A) of the nucleus as $a \approx A/8$ MeV^{-1}. However, there is a significant departure from this liquid drop value at shell closures. This departure is the largest for the doubly magic nucleus ^{208}Pb, where a (at $E_X \sim 7$ MeV) is as low as $A/26$ MeV^{-1}. This shell effect on the NLD parameter is expected to damp with excitation energy so that a approaches its liquid drop value at $E_X \sim 40$ MeV [10]. It is important to make measurements on the damping of the shell effect over a wide E_X range. To our knowledge, no such measurement has been reported.

Experimental information on the damping of the shell effect can be obtained by measuring the E_X dependence of the NLD over a wide range, typically ~5–40 MeV. One method, which is limited to the particle bound excitation energy region, involves the measurement of continuum γ-ray spectra following inelastic scattering and transfer reactions [11]. Both NLD and γ-ray strength function are inputs to the analysis of the spectra. Syed *et al.* used ^{3}He induced inelastic scattering and single nucleon transfer reaction to populate $^{205-208}$Pb [12] and extracted the energy dependence of NLD from the coincident γ spectrum up to $E_X \sim 6$ MeV. Another method of addressing the E_X dependence of NLD over a wider range is by measuring particle evaporation spectra following heavy ion fusion reaction and using a statistical model analysis [13]. Lunardon *et al.* [14] measured proton evaporation spectra in ^{10,11}B + ^{198}Pt reactions and extracted the NLD in ^{208}Pb at an excitation energy ~50 MeV. However, this excitation energy is above the region influenced by the shell effect, and the extracted NLD showed the expected liquid drop behavior. It is indeed difficult to access a much lower excitation energy region using such heavy ion fusion reaction because of the large Coulomb barrier in the entrance channel. One way out of this difficulty is to measure particle evaporation spectra following transfer induced fusion process populating particle unbound states.

In this Letter, we present an exclusive measurement of neutron spectra from ^{208}Pb, following triton transfer in the

^{7}Li + ^{205}Tl reaction, in coincidence with ejectile alpha particles. The nucleus ^{208}Pb (formed in the excitation energy range 19–23 MeV in this work) decays predominately by first step neutron emission populating ^{207}Pb in $E_X \sim 3$–14 MeV. Over this E_X range, the NLD parameter is expected to show a significant change due to the damping of the shell effect. We have also made the above measurement with a ^{181}Ta target populating nuclei in the ^{184}W region where the shell effect is expected to be small.

The experiment was performed at the Mumbai Pelletron Linac Facility using a 30 MeV pulsed ^{7}Li beam of width ~1.5 ns (FWHM) and period ~107 ns. Self-supporting foils of 4.7 mg/cm^2 ^{205}Tl (enriched to >99%) and 3.7 mg/cm^2 ^{181}Ta (~100% natural abundance) were used as targets. Alpha particles were detected at backward angles (~126°–150°) in 8 CsI(Tl) detectors of dimensions 2.5 cm × 2.5 cm × 1 cm (thick) coupled to Si(*P-I-N*) photodiodes and placed at a distance of ~5 cm from the target. The detectors were covered with an aluminized mylar foil of thickness ~1 μm. Particle identification was done using the standard pulse shape discrimination method by measuring the zero crossover timing (ZCT) of the amplified bipolar pulse.

Neutrons were detected using an array of 15 plastic detectors each of dimension 6 cm × 6 cm × 100 cm viewed by two photomultipliers, one at each end [15]. The array was placed at a mean angle of 90° to the beam direction and at a distance of 1 m from the target. The neutron energy was measured using the time of flight (TOF) technique. The data were collected in an event by event mode using a CAMAC based data acquisition system. The parameters recorded were (a) left and right timing of each plastic detector with respect to rf from the beam pulsing system using time to digital converters, (b) integrated charge of anode pulses (which is related to the electron equivalent energy, E_{ee}, deposited in the plastic detector) from the left and right photomultipliers using charge to digital converters, (c) timing of CsI(Tl) detectors with respect to the pulsed beam, (d) energy deposited in the CsI(Tl) detectors (E_{CsI}), and (e) ZCT of the CsI detectors.

A typical ZCT-E_{CsI} 2D spectrum is shown in Fig. 1 displaying a clean separation of various groups of particles. The energy calibration of the CsI(Tl) detectors, in the range $E_\alpha \sim 5$–25 MeV, was done using a ^{229}Th alpha source and the ^{12}C(^{12}C, α)^{20}Ne reaction at $E(^{12}\text{C}) = 24$ MeV populating discrete states in ^{20}Ne. For the latter measurement, the carbon targets, backed by 1–3 mil thick Ta foils, were placed 23 cm upstream of the center of the reaction chamber and the detectors brought to 0° to reduce the kinematic energy spread. The projected alpha energy spectrum for the ^{205}Tl target is shown in the inset of Fig. 1. The calibration of the energy deposited in the plastic detector (in E_{ee}) was done using Compton tagged recoil electrons from ^{137}Cs and ^{60}Co γ-ray sources. The time calibration was done using a precision time calibrator.

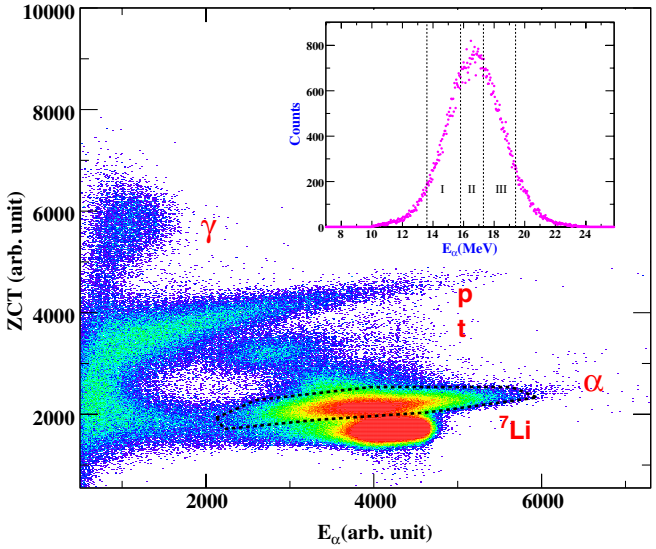

FIG. 1 (color online). Two-dimensional plot of ZCT versus energy deposited in one of the CsI(Tl) detectors in ^{7}Li + ^{205}Tl reaction. The inset shows the projected spectrum of the alpha particles defined by the dotted two-dimensional gate. The vertical lines define three alpha energy bins (see text).

The TOF, position information, and geometric mean of the energy deposited for the neutron events in the plastic detector have been derived as in Ref. [15]. In order to minimize the contribution of scattered neutrons, a TOF dependent energy threshold (increasing with decreasing TOF) was used to obtain the final TOF spectra after subtracting the contribution from the random coincidences. A typical TOF spectrum is shown in Fig. 2. The efficiency of the plastic detector as a function of incident neutron energy and energy threshold was calculated using a Monte Carlo simulation code [15]. The efficiency corrected energy spectra of neutrons were derived from the TOF data.

The neutron energy spectra for the Tl target are shown in Fig. 3(a) for three alpha energy bins, defined in Fig. 1.

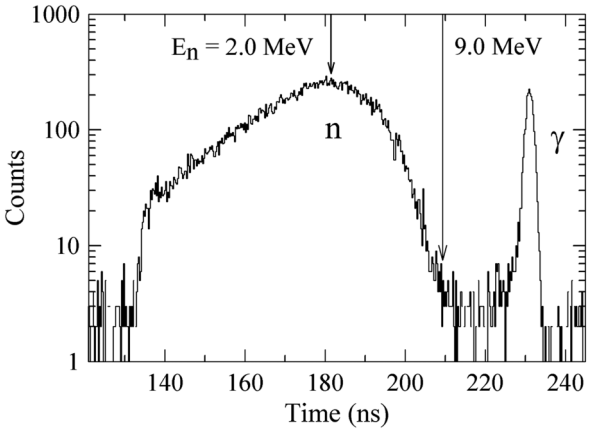

FIG. 2. Time of flight spectrum in ^{7}Li + ^{205}Tl reaction for the central energy bin of alpha particles. The arrows indicate the positions for two representative neutron energies.

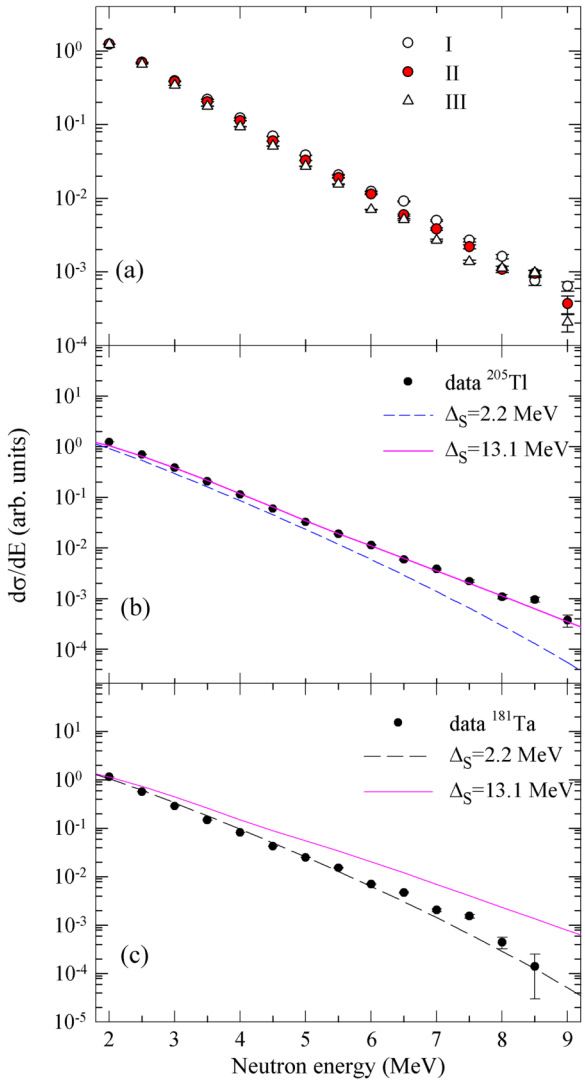

FIG. 3 (color online). (a) Measured neutron spectra from ^{205}Tl target for three alpha bins I, II, III (see Fig. 1). (b), (c) Measured neutron spectra from ^{205}Tl and ^{181}Ta targets and SM calculations for the central alpha energy bin which corresponds to an excitation energy ~21 MeV.

An overall decrease in the slope of the spectra with the increase in alpha energy (implying a decrease of E_X in ^{208}Pb) is consistent with the statistical nature of the neutron decay from an equilibrated nucleus. Figures 3(b) and 3(c) show the energy spectra for both the targets gated by the central alpha energy bin.

The statistical model (SM) analysis of the spectra was done using the code CASCADE [16] with the E_X and J dependent NLD,

$$\rho(E_X, J) = \frac{2J+1}{12\sqrt{a}U^2}\left(\frac{\hbar^2}{2\Im}\right)^{3/2} e^{2\sqrt{aU}},$$

where $U = E_X - E_{\rm rot} - \Delta_P$, Δ_P is the pairing energy, and $E_{\rm rot} = (\frac{\hbar^2}{2\Im})J(J+1)$, $\Im$ being the moment of inertia. The excitation energy dependence of the NLD parameter a, which includes the shell effect and its damping, has been parametrized by Ignatyuk *et al.* [17] as

$$a = \tilde{a}\left[1 - \frac{\Delta_S}{U}(1 - e^{-\gamma U})\right].$$

Here, $\tilde{a}$ is the asymptotic value of the NLD parameter in the liquid drop region, Δ_S is the shell correction energy, which is the difference between the experimental binding energy and that calculated from the LDM, and γ is the damping parameter. Figures 3(b) and 3(c) show the calculated spectra using $\tilde{a} = A/8.5$ MeV^{-1} and $\gamma = 0.055$ MeV^{-1} [18]. It is seen from the figure that a shell correction energy $\Delta_S = 13.1$ MeV (for ^{207}Pb) fits the shape of neutron spectrum for the Tl target while $\Delta_S = 2.2$ MeV does not. An opposite behavior is seen for the Ta target. These values agree with those obtained from the experimental nuclear masses and the calculated LDM values [19]. The present data, therefore, are consistent with the shell correction energies derived from the nuclear masses.

We now address the extraction of the damping parameter from the present data. It may be pointed out that constraining all three parameters, $\tilde{a}$, Δ_S, and γ, is not possible from the data addressing even a much wider excitation energy range. By fixing any two parameters the third one can be constrained. Since the shell correction energy is known with a reasonably good accuracy (within a few hundred keV [19]), we have fixed Δ_S and searched for an acceptable range of $\tilde{a}$ and γ. The shell correction energy was taken as 13.1 and 11.7 MeV for ^{207}Pb and ^{206}Pb, respectively. These two nuclei are only relevant in the present case because the first two steps of neutron emission describe the full spectra.

The calculations were performed with $\delta a (= A/\tilde{a})$ and γ ranging from 6.5–11.0 MeV and 0.02–0.08 MeV^{-1}, respectively. Figure 4(a) shows statistical model fits for the central alpha energy bin for $\delta a = 8.5$ MeV and three γ values. The quality of the fits can also be judged from the ratio plots shown in Fig. 4(b). Whereas a value of $\gamma = 0.060$ MeV^{-1} gives a good fit, the other two values can be discarded. It may be mentioned that a change in shell correction energies up to 0.5 MeV has <2% effect on the shape of the spectra. Similar analysis has been done for the other two alpha energy bins. Figure 5 shows a δa-γ two-dimensional exclusion plot, the region inside the contour representing the acceptable range of parameter values for fitting the present data. The criterion of rejection is based on both the relative χ^2 values and the visual inspection of the fits over a range of $E_n = 2$–9 MeV. It can be seen from the figure that the acceptable range of δa lies between 8.0 and 9.5 MeV. The parameter γ controlling the damping of the shell effect can be constrained to $(0.060^{+0.010}_{-0.020})$ MeV^{-1}. This is different from the value extracted from the neutron resonance data viz. (0.079 ± 0.007) MeV^{-1} [20]. This could be due to the differences in the angular momentum states sampled in

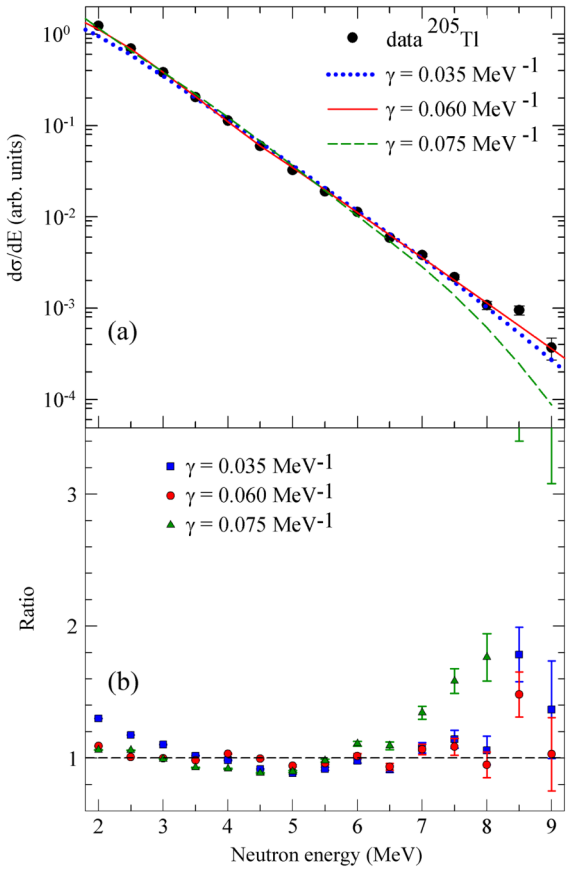

FIG. 4 (color online). (a) Comparison of data with SM calculation using $\Delta_S = 13.1$ MeV (for ^{207}Pb) and 11.7 MeV (for ^{206}Pb) for three values of γ and (b) ratio plot of data to fits for these γ values.

the two works. Moreover, the present work addresses a specific nuclear region whereas the analysis of Ref. [20] is global in character.

Finally, we discuss the possible sources of uncertainties in the present experimental method. While the major contribution to the α-coincident neutron spectra is expected to arise from triton transfer-fusion reaction, there are other direct processes that could contribute. The proton pickup and two-neutron transfer cross sections are small [21] and can be ignored. A Monte Carlo calculation of the alpha-neutron coincidence spectrum reveals that the contribution from the one neutron and one proton transfer is a small fraction ($< 5\%$) in the region of interest, even if the cross sections are the same as that of the main reaction. The most relevant reaction is the deuteron transfer followed by ^{5}He breakup. However, the spectroscopic factor for the $d + {}^5$He configuration is expected to be much smaller than the $t + {}^4$He configuration [22] leading to a small contribution from this reaction.

In conclusion, we have, for the first time, measured the effect of the shell correction on the level density parameter over a range of excitation energy where the

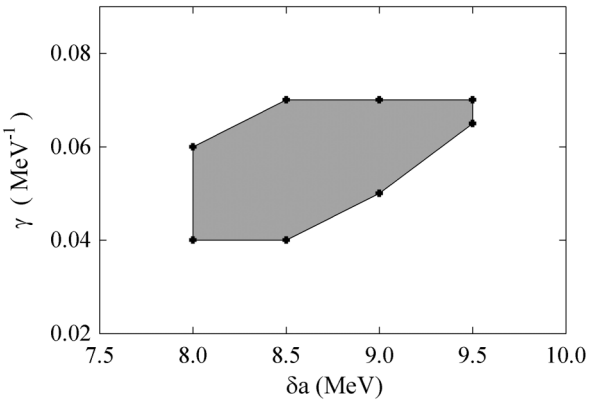

FIG. 5. Exclusion plot of δa-γ, where $\delta a = A/\tilde{a}$, for the shell correction energies quoted in Fig. 4. The acceptable values are within the contour.

effect of damping is significant. The experimental results show that the shell correction is indeed necessary to explain the data and is pronounced in the Pb region. The shell damping factor $\gamma = (0.060^{+0.010}_{-0.020})$ MeV^{-1} has been extracted from the data. A precise measurement of the damping parameter in heavy magic nuclei will be a useful input in the current research on the formation of superheavy nuclei from heavy ion fusion reactions. The precision of the present method can be improved by using a sharper time profile of the pulsed beam, pulse shape discrimination based neutron detectors, and a larger angular coverage.

We thank S. S. Kapoor for his valuable suggestions. We acknowledge the help of the target laboratory staff, the Mumbai Pelletron Linac Facility (PLF) staff for smooth operation of the accelerator, and Nitali Dash, R. Kujur, and M. Pose for their support during the experiment.

*prout@barc.gov.in

[1] Yu. Ts. Oganessian *et al.*, Phys. Rev. Lett. **104**, 142502 (2010).
[2] S. Hofmann and G. Munzenberg, Rev. Mod. Phys. **72**, 733 (2000).
[3] S. M. Polikanov, Usp. Fiz. Nauk **94**, 43 (1968) [Sov. Phys. Usp. **11**, 22 (1968)].
[4] V. M. Strutinsky, Nucl. Phys. **A122**, 1 (1968).
[5] R. V. F. Janssens and T. L. Khoo, Annu. Rev. Nucl. Part. Sci. **41**, 321 (1991).
[6] C. R. Hoffman *et al.*, Phys. Lett. B **672**, 17 (2009).
[7] R. Kanungo *et al.*, Phys. Rev. Lett. **102**, 152501 (2009).
[8] H. A. Bethe, Phys. Rev. **50**, 332 (1936).
[9] A. Bohr and B. R. Mottelson, *Nuclear Structure* (Benjamin, New York, 1969), Vol. 1.
[10] V. S. Ramamurthy, S. K. Kataria, and S. S. Kapoor, Phys. Rev. Lett. **25**, 386 (1970).
[11] E. Melby, L. Bergholt, M. Guttormsen, M. Hjorth-Jensen, F. Ingebretsen, S. Messelt, J. Rekstad, A. Schiller, S. Siem, and S. W. Ødegård, Phys. Rev. Lett. **83**, 3150 (1999).

[12] N. Syed, M. Guttormsen, F. Ingebretsen, A. Larsen, T. Lönnroth, J. Rekstad, A. Schiller, S. Siem, and A. Voinov, Phys. Rev. C **79**, 024316 (2009).
[13] D. Chakrabarty, V. Datar, S. Kumar, E. Mirgule, H. Oza, and U. Pal, Phys. Rev. C **51**, 2942 (1995).
[14] M. Lunardon *et al.*, Eur. Phys. J. A **13**, 419 (2002).
[15] P. C. Rout, D. R. Chakrabarty, V. M. Datar, S. Kumar, E. T. Mirgule, A. Mitra, V. Nanal, and R. Kujur, Nucl. Instrum. Methods Phys. Res., Sect. A **598**, 526 (2009).
[16] F. Puhlhofer, Nucl. Phys. **A280**, 267 (1977).
[17] A. V. Ignatyuk, G. N. Smirenkin, and A. S. Tishin, Sov. J. Nucl. Phys. **21**, 255 (1975).
[18] K.-H. Schmidt, H. Delagrange, J. P. Dufour, N. Cârjan, and A. Fleury, Z. Phys. A **308**, 215 (1982).
[19] W. D. Myers and W. J. Swiatecki, Lawrence Berkeley Laboratory Report No. LBL-36803, 1994.
[20] S. F. Mughabghab and C. Dunford, Phys. Rev. Lett. **81**, 4083 (1998).
[21] M. Dasgupta (private communication).
[22] R. B. Wiringa (private communication); A. K. Jain (private communication).